Mie scattering and the physical mechanisms of sonoluminescence

C. Villarreal, R. Esquivel-Sirvent, and R. Jáuregui
Instituto de Física, UNAM, Apartado Postal 20-364, México, DF 01000, Mexico
(Received 2 August 1999)

We propose an experimental procedure to investigate possible mechanisms for radiation emission in sonoluminescence. Our analysis is based on Mie's theory of light scattering for a coated sphere in an external medium. Depending on the physical mechanism responsible of sonoluminescence, the dielectric constant of the hot spot changes. As a case study we consider the problem of the detection of an inner plasma core in sonoluminescent bubbles. Our results show that polarization measurements of scattered light should discern the presence of a plasma provided that light detectors are fast enough. Extensions to other emission mechanisms are briefly discussed.

PACS number(s): 78.60.Mq, 51.70.+f

Single-bubble sonoluminescence (SBSL) is a challenging and interesting phenomenon exhibiting an unusual energy concentration needed to convert sound into light. From the experimental point of view, several properties of SBSL have been characterized, such as the bubble radius as a function of time, flash light duration, emission spectra, and the dependence of the phenomenon on initial parameters such as the water temperature, driving acoustic pressure, and noble gas content [1–4]. In particular, experimental measurements of the bubble radius $R(t)$ show that few nanoseconds before attaining its minimum value, and prior to the flash emission, the implosion velocity exceeds Mach-4 relative to the gas [4,5]. This suggests the formation of converging shock waves in the bubble. Recent experiments have provided evidence of shock waves launched into the liquid at the bubble's collapse [6]. If shock waves are present, detailed calculations show that part of the gas inside the bubble should concentrate in a central core in a highly ionized state [7–9]. In this model the essential mechanism for light emission is Bremsstrahlung. However, alternative theories may also account for the intensity and spectral distribution of the radiation emitted during SL: black-body radiation arising from compressional waves [10], energy liberation associated to imploding water jets in the bubble [11], radiation due to proton tunneling in an ice VI shell surrounding the bubble [12], or the disputed application of dynamic Casimir effect to SL [13–16].

To distinguish between the models and find out more about SL, key characteristics of the phenomenon still remain to be determined experimentally: the size of the hot spot, the actual temperatures of the system, the spatial distribution of the radiation emitters, the spectrum beyond the water window, etc. Several proposals have been put forth to investigate some of these characteristics, such as measuring angular intensity correlations of SL flashes to determine isotropy properties of the radiation [17] or to use Thomson scattering techniques [18] to search for free electrons. One widely used method to determine the evolution of the bubble radius is Mie's scattering [4,19]. The standard Mie's technique consists on measuring the intensity of laser light scattered by a bubble. In the short wavelength limit $[\lambda \ll R(t)]$ the size of a homogeneous bubble is inferred from the fact that the scattering is proportional to $R^2(t)$. The scattered intensity depends crucially on the dielectric constants of the gas and fluid at bubble's interface. Our proposal is to use Mie's scattering to detect changes in the dielectric function of the system associated to possible emission mechanisms, for example, the formation of an inner plasma core in SL bubbles, the generation of an ice shell around the bubble, or properties of SL under the application of magnetic fields.

In this paper we will focus on the particular problem of detecting a plasma during SL, through a straightforward application of Mie's theory for coated spheres. Here, the system is assumed to be composed of two concentric spheres embedded in an external infinite medium, each one characterized by its respective dielectric function $\epsilon_i, i=1,2,3$. For definiteness, we will study a model of a pure argon SL bubble in water. Thus, our SL bubble model consists of an inner plasma core $[\epsilon_1 \equiv \epsilon_1(\omega)]$, surrounded by a sphere of less dense almost nonionized Ar $(\epsilon_2 \sim 1)$ [20] embedded in water ($\epsilon_3 = 1.768$, for visible light) [24]. In order to calculate $\epsilon_1(\omega)$ we use the results of numerical simulations of the system dynamics during SL. According to Refs. [7,8,19] shock waves may be generated inside the collapsing SL bubble, yielding a ionization up to fifth order of the Ar atoms, and temperatures up to $T \sim 1 \times 10^5$ K [9]. The subsequent recombination process makes the plasma phase last less than one nanosecond. During this time, the electronic density $N_e \sim 1.0 \times 10^{22}$ cm^{-3} is almost uniformly concentrated in a core of $\sim 1/5$ of the minimum bubble radius; singly ionized atoms mostly fill out this core with a slight tendency to avoid the center of the bubble, while less abundant highly ionized atoms concentrate in a smaller core of about 0.05 μm. However, the system keeps local neutrality at every point. The existence of local thermodynamic equilibrium of the bubble's contents is generally assumed; this is important in building a model of the dielectric function, since it is possible to assign the same local temperature to electrons and ions. Within such approximation the dielectric function of the plasma depends only on the electron density N_e, the ion density $N_i \sim N_e$, and the ion-electron temperature T. For typical experimental plasmas in the absence of an external magnetic field, the complex dielectric function for

 ©2000 The American Physical Society

transverse electromagnetic waves with angular frequency ω is [21]

$$[\epsilon(\omega,T)]^2=1-\frac{\omega_p^2}{\omega(\omega+i\nu_{\rm eff})}, \tag{1}$$

where the plasma frequency ω_p is given by

$$\omega_p^2=\frac{4\pi e^2 N_e}{m_e}, \tag{2}$$

with e and m_e being the electron's charge and mass, and the effective ion-electron collision frequency $\nu_{\rm eff}$ is

$$\nu_{\rm eff}=Z^2\frac{e^4}{m^2}\left(\frac{2\pi m}{3kT}\right)^{3/2}N_i g(\nu,T). \tag{3}$$

Here Z is the charge of the ions, m their mass, and $g(\nu,T)=(\sqrt{3}/\pi)\ln\Lambda$ is the Gaunt factor which, following Ref. [21] is given by

$$\Lambda=\left(\frac{2}{\gamma}\right)^2\frac{1}{e'^{1/2}}\left(\frac{kT}{m}\right)^{1/2}\frac{kT}{Ze^2\omega_p} \tag{4}$$

with $\gamma\approx 1.781$ and $e'\approx 2.718$. This expression is considered valid for $\omega_p\leqslant\omega$, and $T\leqslant 4Z^2\times 10^5$. For SBSL parameters, $\omega_p\sim 5.6\times 10^{15}$ Hz so that, for optical frequencies, the Gaunt factor Eq. (4) is $g(\nu,T)\sim 1$, and $\nu_{\rm eff}\sim 1\times 10^{15}$. Two typical wavelenghts ($\lambda=2\pi c/\omega$) employed in Mie scattering SL experiments are $\lambda=637$ nm (red light) and $\lambda=410$ nm (blue light). From Eq. (1) the resulting dielectric constants associated to these wavelengths are $\epsilon_1=-2.21+1.08i$ and $\epsilon_1=-0.42+0.31\ i$, respectively. The scattered electric fields for a plane transverse electromagnetic wave incident upon a coated sphere are given by [22,23]

$$E_\perp^s=\left(\frac{-i}{k_3R}\right)E_\perp^o\exp(ik_3R)S_\perp\,, \tag{5}$$

$$E_\parallel^s=\left(\frac{i}{k_3R}\right)E_\parallel^o\exp(ik_3R)S_\parallel\,, \tag{6}$$

where $k_i=\sqrt{\epsilon_i}2\pi/\lambda$ is the wave number in region i and

$$S_\perp=\sum_{n=1}^{\infty}\frac{2n+1}{n(n+1)}\left[a_n^s\frac{P_n^1(\cos\theta)}{\sin(\theta)}+b_n^s\frac{dP_n^1(\cos\theta)}{d\theta}\right], \tag{7}$$

$$S_\parallel=\sum_{n=1}^{\infty}\frac{2n+1}{n(n+1)}\left[a_n^s\frac{dP_n^1(\cos\theta)}{d\theta}+b_n^s\frac{P_n^1(\cos\theta)}{\sin(\theta)}\right]. \tag{8}$$

The subindexes $\perp$ and $\parallel$, refer to the transverse and parallel components of the electric field with respect to the scattering plane, and the parameters $a_n^s(k_1,k_2,k_3)$ and $b_n^s(k_1,k_2,k_3)$ are *effective* Mie coefficients for the case of two concentric scattering interfaces [23]. The scattering cross sections are directly found from $d\sigma/d\Omega=I/I_0$, where $I=c/8\pi|E|^2$ is the intensity of the scattered field. The total scattering cross section is

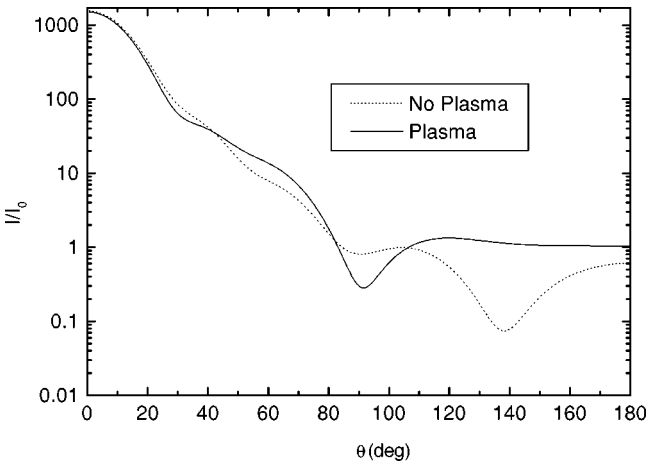

FIG. 1. Differential scattering cross section for red light scattered from a $R=0.6\ \mu$m bubble with a plasma core (dotted line) and without it (solid line).

$$\sigma=\frac{\pi}{k^2}\sum\ (2n+1)(|a_n|^2+|b_n|^2). \tag{9}$$

In Fig. 1 we present the differential scattering cross section $d\sigma/d\Omega$ for red light scattered by a bubble at the time of SL with a radius of $R=0.6\ \mu$m. We compare the cases with a plasma core present [plasma bubble (PB)] or absent [no plasma bubble (NPB)]. The differential scattering cross section integrated in forward directions basically coincides. Indeed, the total scattering cross sections are $\sigma_{\rm PB}=0.12\ \mu{\rm m}^2$, and $\sigma_{\rm NPB}=0.13\ \mu{\rm m}^2$, respectively. Therefore, measurements of the bubble radius based on Mie's scattering [4] will yield approximately the same results within this angular region, regardless of the presence of the plasma core. For angles $\theta\geqslant 90°$ we observe that the PB scatters less light than the NPB, while the converse is true for $\theta\sim 140°$. However, detailed calculations show that the structure of $d\sigma/d\Omega$ for $\theta\geqslant 90°$ is more sensitive to variations associated to the specific characteristics of the model under consideration, e.g., on the relative radii of the plasma core and bubble at the time of SL, on the choice of the dielectric constant for the radiant material, on the plasma dynamics, etc. Therefore, a search of the plasma core requires a theoretical-experimental approach based on the careful analysis of other complementary measurements such as polarization of the scattered light, comparison of the cross section for different wavelengths, as well as more precise determinations of the radius at the emission time. As a definite plasma diagnosis scheme, we propose a relative scattering technique based on the comparison of either polarized or unpolarized measurements of the light scattered by a reference NPB with that scattered by a smaller PB or NPB. Thus, we define the relative scattering measurement as

$$\Delta_q(R_j,R_i)=\frac{\sigma_q(R_j)-\sigma_q(R_i)}{\sigma_q(R_j)}, \tag{10}$$

where $\sigma_q(R_i)$ refers to the differential scattering of a bubble of radius R_i (in microns) for scattered light of polarization q. If no subindex appears, the cross section is related to unpolarized measurements. As a reference bubble we choose an

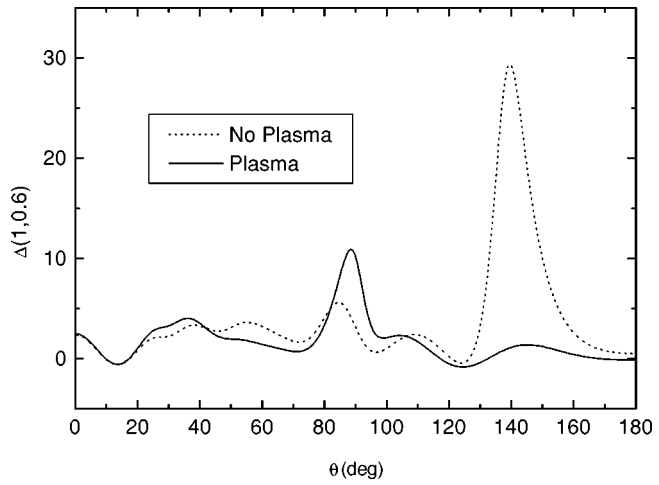

FIG. 2. Relative scattering cross section for unpolarized red light. When no plasma is present (solid line) a marked peak appears at $\theta\sim 140°$, while for the plasma case a smaller peak appears at $\sim 90°$. These peaks are reminiscent of the structure of the differential scattering cross section (Fig. 1).

NPB of radius $R_o = 1\ \mu$m, given that an argon bubble in water does not luminesce at this radius according to both theoretical [9] and experimental results [4].

As an example, we present in Figs. 2–4 the structure of $\Delta(1.0,0.6)$ for 637 nm light. For unpolarized light detection, we observe in Fig. 2 a definite difference between the maxima of Δ for PB and NPB at $\theta\sim 90°$, and a marked peak for NPB at $\theta\sim 140°$. This is a reminiscence of the fact that at $\theta\sim 90°$ a PB scatters less light than an NPB, while at $\theta \sim 140°$ the former scatters more. These observations are valid also when $0.8\leqslant R_i\leqslant 1.0$ and $0.5\leqslant R_j\leqslant 0.6$. In this sense, these results are robust under changes of the possible radii at which SL occurs. The aforementioned structure can be enhanced and better discriminated with the help of polarization measurements. For parallel polarization (Fig. 3) the PB maximum at $\theta\sim 90°$, increases 60 times, whereas the

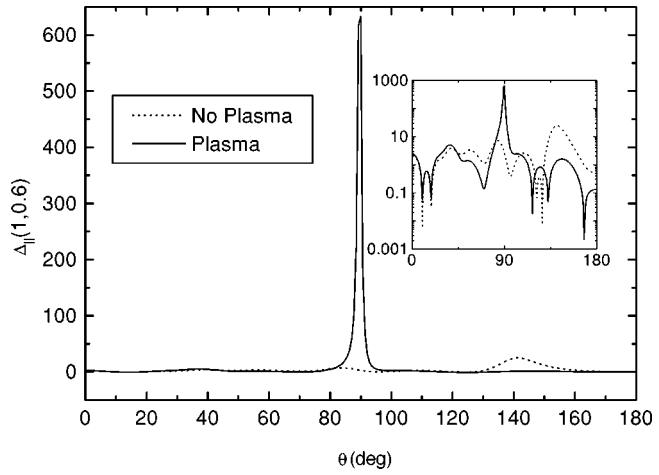

FIG. 3. Relative scattering cross section for parallel polarized red light. For the bubble with a plasma core the peak at $\theta\sim 90°$ increase by a factor of 60, compared to the unpolarized case (Fig. 2). The NPB peak at $\theta\sim 140°$ remains the same as for the unpolarized case. The inset, in logarithmic scale shows the details of $\Delta_\parallel$ with and without plasma.

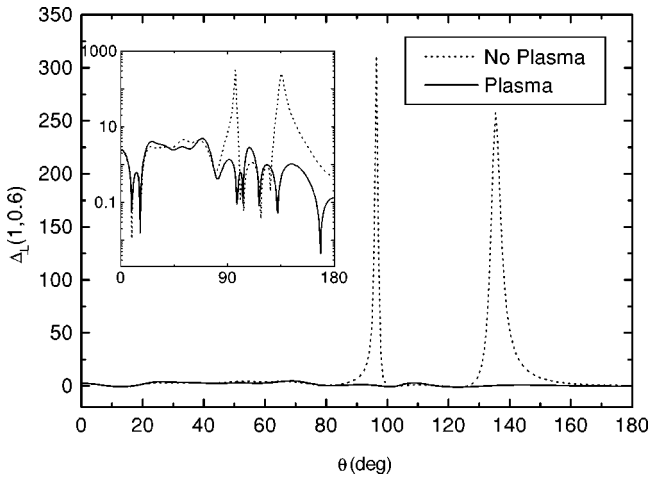

FIG. 4. Relative scattering cross section for transverse polarized red light. The PB peak at $\theta\sim 90°$ is absent and instead, the NPB (dotted line) shows two prominent peaks at $\theta\sim 95°$ and PB and NPB cases.

NPB maximum at $\theta\sim 140°$ remains basically the same. Noteworthy, a reversed pattern is observed for transverse polarization (Fig. 4), where the PB peak at $\theta\sim 90°$ disappears, while the NPB curve shows two prominent peaks at $\theta\sim 95°$ and at $\theta\sim 140°$. The latter is shifted by about 5° and increases its amplitude by a factor of 10. The contrasting role of the PB and NPB peaks for each polarization would be a clear confirmation of the existence or absence of the plasma core in a sonoluminescent bubble.

The former analysis can be applied to different wavelengths of the scattered light. In the particular case of blue (410 nm) light, the structure of the relative scattering function for unpolarized light is very similar to the discussed above, except that the position of the first peak (associated to a PB) is shifted to higher angles $\theta\sim 110°$, while the position of the second one (associated to a NPB) remains unchanged. Again, this structure can be further analyzed with the help of polarization measurements. The strongest signature of a PB is that the first peak increases its amplitude dramatically for parallel polarization.

In conclusion, for the particular model worked out in this paper, one clear evidence of a plasma core would be the great difference between parallel and transverse polarized scattered light between the reference bubble and the SL bubble for angles $\theta\geqslant 90°$. Another evidence would be the absence or presence of a strong NPB peak at $\theta\sim 140°$. It is worthwhile to mention that although we focused on the SL plasma model, we also studied the ice VI core model recently proposed by Willison [12]. Using the refractive index for ice VI, $n = 1.46$, obtained by means of the semiempirical formula of Thormälen *et al.* [24], the total scattering cross section for the ice coated bubble would be similar to that scattered from a $R\sim 10\ \mu$m air bubble. This would be easily detectable as a sudden and strong discontinuity in the total scattered intensity.

The results presented in this paper are proper of the specific model discussed here; however, the actual experimental realization should provide similar patterns, with possible changes in the amplitude and position of the peaks arising-from the relative scattering measurements. This approach can

be supplemented by considering the application of magnetic fields. Upon the action of strong magnetic fields, the associated dynamics of charged particles may induce different spatial distributions of the plasma, with consequent anisotropic properties of the dielectric constant. The implementation of this technique seems straightforward provided that the light detectors are fast and sensitive enough to measure the intensity of backscattered light at the precise time of SL.

The authors thank Professor R. Barrera for helpful discussions and CONACYT J27710-T.

[1] B.P. Barber and S.J. Putterman, Nature (London) **352**, 318 (1991).
[2] R. Hiller, K. Weninger, S.J. Putterman, and B.P. Barber, Science **266**, 248 (1994).
[3] K. Weninger, R. Hiller, B.P. Barber, D. Lacosteand, and S.J. Putterman, J. Phys. Chem. **99**, 14 195 (1995).
[4] B. Barber, R.A. Hiller, R. Lofstedt, S. Putterman, and K. Weninger, Phys. Rep. **281**, 67 (1997).
[5] K.R. Weninger, B.P. Barber, and S.J. Putterman, Phys. Rev. Lett. **78**, 1799 (1997).
[6] J. Holzfuss, M. Ruggeberg, and A. Billo, Phys. Rev. Lett. **81**, 5434 (1998).
[7] C.C. Wu and P.H. Roberts, Phys. Rev. Lett. **70**, 3424 (1993).
[8] L. Kondic, J.I. Gersten, and C. Yuan, Phys. Rev. E **52**, 4976 (1995).
[9] N. Xu, L. Wang, and X. Hu, Phys. Rev. E **57**, 1615 (1998).
[10] H.Y. Cheng, M.C. Chu, P.T. Leung, and L. Yuan, Phys. Rev. E **58**, R2705 (1998).
[11] A. Prosperetti, J. Acoust. Soc. Am. **101**, 2003 (1997).
[12] J.R. Willison, Phys. Rev. Lett. **81**, 5430 (1998).
[13] J. Schwinger, Proc. Natl. Acad. Sci. USA **90**, 2105 (1993); **90**, 7285 (1993).
[14] C. Eberlein, Phys. Rev. Lett. **76**, 3842 (1996).
[15] R. Esquivel-Sirvent, R. Jáuregui, and C. Villarreal, Phys. Rev. A **56**, 2463 (1997).
[16] K.A. Milton and Y.J. Ng, Phys. Rev. E **55**, 4207 (1997).
[17] Y. Hama, T. Kodama, and S.S. Padula, Phys. Rev. A **56**, 2233 (1997).
[18] S. Putterman, Phys. World **5**, 38 (1998).
[19] W.J. Lentz, A.A. Atchley, and D.F. Gaitan, Appl. Opt. **34**, 2648 (1995).
[20] I.Sh. Model, Sov. Phys. JETP **5**, 589 (1957).
[21] V.L. Ginzburg, *Propagation of Electromagnetic Waves in a Plasma* (Gordon and Breach, New York, 1961).
[22] P.J. Brussard and H.C. van de Hulst, Rev. Mod. Phys. **34**, 507 (1962).
[23] A. Aden and M. Kerker, J. Appl. Phys. **22**, 1242 (1951).
[24] I. Thormahlen, J. Straub, and U. Grigull, J. Phys. Chem. Ref. Data **14**, 933 (1985).